

Equilibrium Properties of Double-Screened-Dipole-Barrier SINIS Josephson Junctions

Branislav K. Nikolić,¹ J. K. Freericks,¹ and P. Miller²

¹*Department of Physics, Georgetown University, Washington, DC 20057-0995*

²*Department of Physics, Brandeis University, Waltham, MA 02454*

We report on a self-consistent microscopic study of the DC Josephson effect in *SINIS* junctions where screened dipole layers at the *SN* interfaces generate a double-barrier multilayered *SIN* structure. Our approach starts from a microscopic Hamiltonian defined on a simple cubic lattice, with an attractive Hubbard term accounting for the short coherence length superconducting order in the semi-infinite leads, and a spatially extended charge distribution (screened dipole layer) induced by the difference in Fermi energies of the superconductor *S* and the clean normal metal interlayer *N*. By employing the temperature Green function technique, in a continued fraction representation, the influence of such spatially inhomogeneous barriers on the proximity effect, current-phase relation, critical supercurrent and normal state junction resistance, is investigated for different normal interlayer thicknesses and barrier heights. These results are of relevance for high- T_c grain boundary junctions, and also reveal one of the mechanisms that can lead to low critical currents of apparently ballistic *SNS* junctions while increasing its normal state resistance in a much weaker fashion. When the *N* region is a doped semiconductor, we find a substantial change in the dipole layer (generated by a small Fermi level mismatch) upon crossing the superconducting critical temperature, which is a new signature of proximity effect and might be related to recent Raman studies in Nb/InAs bilayers.

PACS numbers: 71.27.+a, 74.50.+r, 74.80.Fp, 73.40.Jn

I. INTRODUCTION

The Josephson effect¹ is one of the most spectacular phenomena arising from the macroscopic phase coherence of Cooper pairs. A dissipationless current flows at zero voltage between two superconductors weakly coupled through a tunnel barrier (*SIS*, where *S* and *I* denote a superconductor and an insulating barrier, respectively) or weak links (*ScS*, *SNS*, etc., where *c* stands for a constriction, and *N* for a normal metal). The study of such inhomogeneous superconducting structures has been driven by both interest in the fundamentals of quantum mechanics, and by the potential application of Josephson junctions as circuit elements in electronic devices.²

Recently, considerable attention has been directed toward the study of *SINIS* junctions,^{3–5} where the insulating tunnel barrier is split into two pieces separated by a normal metal. These types of junctions have provided a playground to study the interplay⁶ between the mesoscopic coherence of a single-particle wave function in the normal metal and the macroscopic coherence of a many-body wave function of Cooper pairs.⁷ Furthermore, the reexamination of various multilayered structures of the *SINIS* type in applied research has been driven by the struggle to optimize the performance of Josephson junctions in low-temperature superconducting (LTS) digital electronics.^{8–10} In mesoscopic superconductivity, one frequently deals with *S-Sm-S* junctions³ (*Sm* being a heavily doped semiconductor with a two-dimensional electron gas) where the role of the *I* layer is played by a space-charge layer arising at the *S-Sm* interface (additional scattering at the interface can occur from the mismatch

between the effective electron masses and Fermi momenta in the *S* and *Sm*). The technological advances in fabricating such hybrid structures³ have given an impetus to the field of mesoscopic superconductivity^{6,7} where the two-dimensional electron gas is amenable to an engineering of its “metallic” properties; i.e., one can tune the Fermi wavelength, or mean free path, and one can confine electrons with gate electrodes. In such structures, phase-coherence of the electron and Andreev-reflected hole¹¹ at the *SN* interface can be studied without too much normal reflection, because the charge-accumulation layer arising at a typical Nb/InAs interface, or the Schottky barrier at a Nb/Si interface, are much more transparent than typical dielectric tunnel barriers.⁶

While initial understanding of the Josephson effect came from studies of tunnel junctions,¹ further developments concentrated on weak links¹² which provide the non-hysteretic (i.e., single valued) $I - V$ characteristic needed for applications, like SQUIDs¹³ or rapid single flux quantum logic.¹⁴ The return to *SIS* junctions came after the fabrication of Nb/Al tunnel junctions¹⁵ with a reliable control of the critical current (conventional tunnel junctions can be made non-hysteretic by externally shunting their high capacitance with a resistor, which reduces the overall performance¹⁶). The renewed interest⁹ in *SINIS* multilayered junctions for LTS electronics comes from an attempt to combine the advantageous properties of both weak links and tunnel junctions⁸—the *SINIS* junctions are intrinsically shunted, while exhibiting large characteristic voltages with moderate critical current densities (in fact, rapid single flux quantum devices require large critical current densities, to reduce the error rate,¹⁴ which is difficult to achieve using standard

$\text{Nb}/\text{Al}/\text{AlO}_x/\text{Nb}$ tunnel junction technology, but might be reached in *SINIS* junctions with carefully engineered properties⁹). When the N interlayer is clean, the junction resistance is mainly controlled by scattering at the interfaces (like in conventional $\text{Nb}/\text{Al}/\text{AlO}_x/\text{Al}/\text{Nb}$ junctions¹⁷), and not by the interlayer material properties.

Here we undertake a study of a special class of *SINIS* junctions where the double-barrier structure arises from two inhomogeneous screened dipole layers (SDL) determined by a relatively large Debye screening length l_D of a few lattice spacings. We start from a microscopic lattice Hamiltonian with the S and N layers described by different metals that have the same bandwidth, but their Fermi levels are misaligned. The Fermi level mismatch forces a charge redistribution, with the strongest deviation from uniformity located near the SN interface, which is gradually diminished inside the bulk layers on a length scale set by l_D . The charge profile ensures an equilibration of the chemical potential throughout the system when no bias voltage is applied. Since we assume a screening length of a few lattice spacings, the dipole layer is spatially extended (i.e., thicker than just one monoatomic layer). This choice of microscopic junction parameters allows us to examine the charge redistribution appearing between conductors which are less efficient in screening than ordinary metals (such as the underdoped cuprates or InAs). Our treatment of the double SDL barrier is fully microscopic and self-consistent, meaning that effects of the static electric potential (generated by the excess charge) on the Josephson current and on the normal state resistance are related to the parameters of the underlying Hamiltonian, rather than characterizing the barrier by an effective transparency^{4,10,20} D , or using a delta function potential at the SN interface to model the normal reflection^{21,22} (in addition to the inevitable retroreflection¹¹). We tackle both the fundamental aspects of the problem (like the self-consistent evaluation of the order parameter, the change of its phase across the junction, and the emergence of non-sinusoidal current-phase relations) and issues relevant for applications (like the characteristic voltage, a product of the critical current I_c and the normal state resistance R_N , which determines the high-frequency performance of the junction). Our junctions are three-dimensional (3D) and clean, so that quasiparticle transport through the N interlayer is ballistic.

Previous theoretical work on ballistic *SINIS* junctions focused on resonant supercurrents in low-dimensional structures.^{22–25} Mesoscopic superconductivity coherence effects in 3D junctions (e.g., a current proportional to D of the barrier, rather than the characteristic D^2 dependence for two uncorrelated sequential tunneling processes) have been investigated in Ref. 4. These junctions are mostly similar to the ones studied here, except that our “microscopic” charge accumulation barriers are not atomically sharp interfaces that can be described by a phenomenological transparency D . A more microscopic treatment of the effect of charge inhomogeneity for

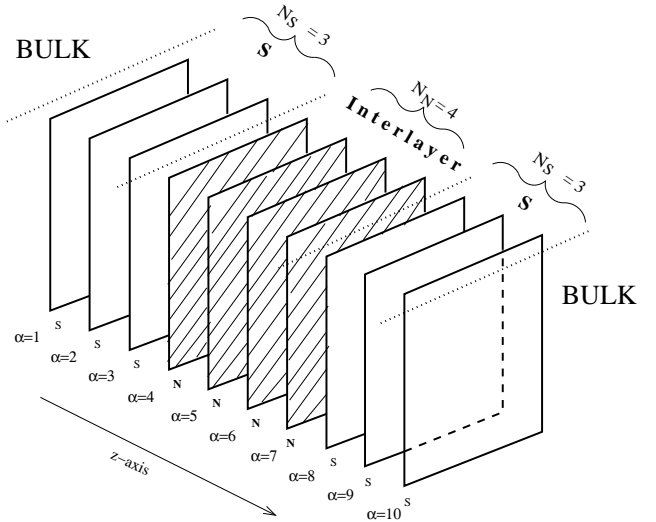


FIG. 1. Microscopic stacked planar geometry of a Josephson junction defined on an infinite simple cubic lattice with a lattice constant a . The normal interlayer contains N_N planes (ranging from 1 to 60) which are coupled to semi-infinite superconducting leads (the junction thickness is $L = N_N a$). These layers, together with the first N_S planes (30 in our calculations) in each lead, comprise the region of the junction where the self-consistent calculation is performed. The junction is allowed to have spatial inhomogeneity only within the $2N_S + N_N$ modeled planes, but the calculations are for an infinite system. The insulating barriers are formed by a charge redistribution that is localized near the SN interfaces.

normal transport through the contact of two different metals (a problem frequently appearing in the multilayers of giant magnetoresistance devices²⁶) has been undertaken using the Boltzmann equation,²⁷ and in superconducting junctions using quasiclassical methods in a non-self-consistent fashion.²⁸ It is worth emphasizing that standard quasiclassical Green function techniques, which exploit the fact that macroscopic quantities vary on a length scale substantially exceeding the interatomic distance, cannot be applied directly to problems containing boundaries between two different metals. Since electron reflections lead to fast spatial variations of the original Green functions around the boundary, the method has to be extended properly to take this into account (see Ref. 28 for details).

Our study is relevant for three types of recently explored experimental systems: (i) grain boundary junctions²⁹ in high- T_c superconductors, where our short coherence length superconductor and the poor screening of the excess charge (i.e., Debye screening length comparable to the coherence length), mimic the effect of a charge imbalance at the grain boundaries on the depression of the order parameter, and thereby the intergranular current density^{30,31} (without complicating the problem further with d -wave symmetry); (ii) Raman scatter-

ing studies³² of the proximity effects in Nb/InAs hybrid structures reveal a substantial change of the charge accumulation layer formed at such interface above and below the T_c of Nb—we also find that I layer induced by a small Fermi level mismatch is modified by proximity effects in our *SINIS* junctions when the carrier concentration in the N is 100 times smaller than in the S ; (iii) recent experiments on ballistic *SNS* junctions,³³ in the limit where I_c and R_N do not depend on the thickness of the N , exhibit a much smaller characteristic voltage than predicted for short clean *ScS* junctions—the scattering off a dipole charge layer is an example of a process which sharply reduces I_c , but only weakly increases R_N .

The paper is organized as follows. In Sec. II we introduce the model and the main ideas of the Green function computational technique (employed to solve the quantum problem of the charge distribution and equilibrium transport; the electrostatic problem of the potential generated by these charges is solved classically). Section III contains the results for the self-consistent pair amplitude (or the order parameter) and the local change of the phase across the junction. The current-phase relation for different strengths of the electrostatic potential generated by the SDL is discussed in Sec. IV, where we also evaluate the characteristic voltage $I_c R_N$. We conclude in Sec. V.

II. MODELING A *SINIS* JUNCTION WITH A DOUBLE-BARRIER SCREENED DIPOLE LAYER

Early studies of the Josephson effect in *SINIS* junctions were based on a tunneling Hamiltonian formalism and perturbation theory in the barrier transmissivity.¹⁸ Later on, quasiclassical Green function techniques¹⁹ were applied to a double-barrier junction with the N interlayer in the dirty limit.²⁰ While these results are valid only in a few limiting cases, a recent reexamination of this problem covers a wider range of parameters.^{4,9} For example, when transport through the N interlayer is ballistic (mean free path greater than the thickness of the junction), one cannot use standard tools²⁰ like the Usadel equation. Instead, a solution of the Gor'kov equations for the Green functions of the double-barrier structure is required.^{4,10} Furthermore, if the I barriers are not of low transparency, the usual arguments for the validity of rigid boundary conditions¹² (i.e., taking the gap Δ to be constant inside the superconducting leads) fail when the S and N regions have the same cross section, and the thickness of the junction is not much larger than the superconducting coherence length ξ_0 . In such cases, the critical current density can be close to the bulk critical current density, and a self-consistent evaluation of the order parameter inside the S is needed to ensure current conservation throughout the structure.^{34–36} Since we choose to work with a short coherence length superconductor, quasiclassical approximations neglecting dynamics on a length scale below ξ_0 are not applicable (in

our case $\xi_0 \approx 4a$ is not much larger than the Fermi wavelength $\lambda_F \approx 2a$, and spatial variation of the order parameter Δ on a length scale smaller or comparable to ξ_0 is important).

Our approach to quantum transport in ballistic *SINIS* junctions starts from a microscopic Hamiltonian defined on a simple cubic lattice (of lattice constant a).³⁴ It allows us to describe the transport for an arbitrary junction thickness, temperature, and barrier strength. Also, the geometry is such that the N interlayer has the same width as the S leads. For computational purposes, the infinite lattice which models the junction is divided into a self-consistent part and a bulk part, as shown in Fig. 1. A negative- U Hubbard term is employed to model the real-space pairing of electrons due to a local instantaneous attractive interaction.^{34,37} The lattice Hamiltonian is given by

$$H = \sum_{i\sigma} V_i c_{i\sigma}^\dagger c_{i\sigma} - \sum_{\langle ij\sigma \rangle} t_{ij} c_{i\sigma}^\dagger c_{j\sigma} + \sum_i U_i \left(c_{i\uparrow}^\dagger c_{i\uparrow} - \frac{1}{2} \right) \left(c_{i\downarrow}^\dagger c_{i\downarrow} - \frac{1}{2} \right), \quad (1)$$

where $c_{i\sigma}^\dagger$ ($c_{i\sigma}$) creates (destroys) an electron of spin σ at site i , t_{ij} is the hopping integral between nearest-neighbor sites i and j (energies are measured in units of t), which is taken to be the same in the S and N , and $U_i < 0$ is the attractive Hubbard interaction for sites within the superconducting planes. The normal interlayer is described by the noninteracting part of the Hamiltonian (1), which is just a (clean) nearest-neighbor tight-binding model with a diagonal on-site potential V_i . The potentials V_i are not given *a priori*, but instead are calculated self-consistently by first determining the local electronic charge density and comparing it to the bulk charge density of the corresponding S or N layers. The imbalanced charge on each plane generates an electric field and thereby an electric potential. Summing the contributions from the charges on all other planes then yields the total local potential V_i^C and the local potential energy shift $V_i = eV_i^C$. We now recalculate the charge density on each plane and iterate until V_i is determined self-consistently (see below for a detailed description of the algorithm). The local potentials V_i are largest near the SN interface, and decay as one approaches the bulk leads.

We use the Hartree-Fock approximation (HFA) for the interacting part of the Hamiltonian (1). This accounts for the superconductivity in the S region in a way which is completely equivalent to a conventional BCS theory with an energy cutoff determined by the electronic bandwidth rather than by the phonon frequency. We choose half-filling $n_S = 1$ and $U_i = -2$ on the sites in the superconducting leads. The homogeneous bulk superconductor has a transition temperature $T_c = 0.11$ and a zero-temperature order parameter $\Delta = 0.198$. This yields a standard BCS gap ratio $2\Delta/(k_B T_c) \approx 3.6$ and a short

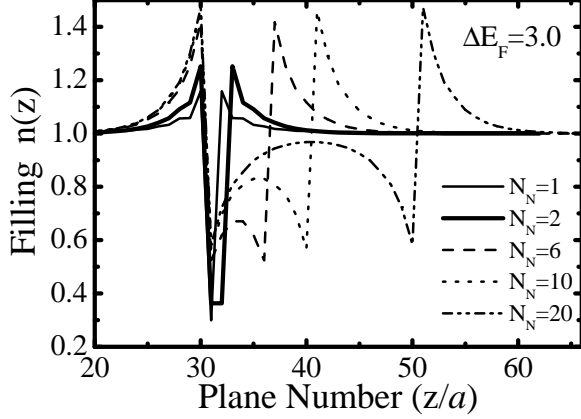


FIG. 2. Scaling of the local density of electrons with the thickness $L = N_N a$ of SINIS Josephson junctions. The filling is the same at each site within the planes (plane number one is the first plane along the z -axis inside the self-consistent region from Fig. 1). The difference in Fermi energies of the S and N is $\Delta E_F = 3.0$. The bulk equilibrium value of the charge density is set to half-filling in both the S and N ($n_S = n_N = 1$). The inhomogeneous charge redistribution is (approximately) symmetric around the SN interface only for a thick enough junction. In the case of a thin junction, the charge is depleted in the N interlayer to lie below half-filling since the screening length is a few lattice spacings.

coherence length $\xi_0 = \hbar v_F / (\pi \Delta) \simeq 4a$. The bulk critical current per unit area a^2 is $I_c^{\text{bulk}} = 1.09 e n \Delta / \hbar k_F$, which is a bit higher than the current density determined by the Landau depairing velocity $v_d = \Delta / \hbar k_F$. This stems from the possibility of having gapless superconductivity in 3D at superfluid velocities slightly exceeding⁴² v_d (note that k_F is direction-dependent for a cubic lattice at half-filling; we use the average value over the Fermi surface $k_F \approx 2.8a$, appearing in the transport formulas, to compare our critical bulk supercurrent density to the expressions that assume a spherical Fermi surface and a density of particles $n = k_F^3 / 3\pi^2$). The junction properties are studied here in the low-temperature limit at $T = 0.01 = 0.09 T_c$ (the BCS gap is essentially temperature independent below $0.6 T_c$). At this temperature, the coherence length of the clean normal metal is $\xi_N = \hbar v_F / 2\pi kT \simeq 40a$. Since we do not consider inelastic scattering processes, the dephasing length L_ϕ is larger than ξ_N . Therefore, $\min(\xi_N, L_\phi) = \xi_N$ determines the coherence properties of a single quasiparticle wave function inside the normal region.

The inhomogeneous superconductivity problem is solved by employing a Nambu-Gor'kov matrix formulation for the Green function $\hat{G}(\mathbf{r}_i, \mathbf{r}_j, i\omega_n)$ between two lattice sites \mathbf{r}_i and \mathbf{r}_j at the Matsubara frequency $i\omega_n = i\pi T(2n+1)$,

$$\hat{G}(\mathbf{r}_i, \mathbf{r}_j, i\omega_n) = \begin{pmatrix} G(\mathbf{r}_i, \mathbf{r}_j, i\omega_n) & F(\mathbf{r}_i, \mathbf{r}_j, i\omega_n) \\ \overline{F}(\mathbf{r}_i, \mathbf{r}_j, i\omega_n) & -G^*(\mathbf{r}_i, \mathbf{r}_j, i\omega_n) \end{pmatrix}. \quad (2)$$

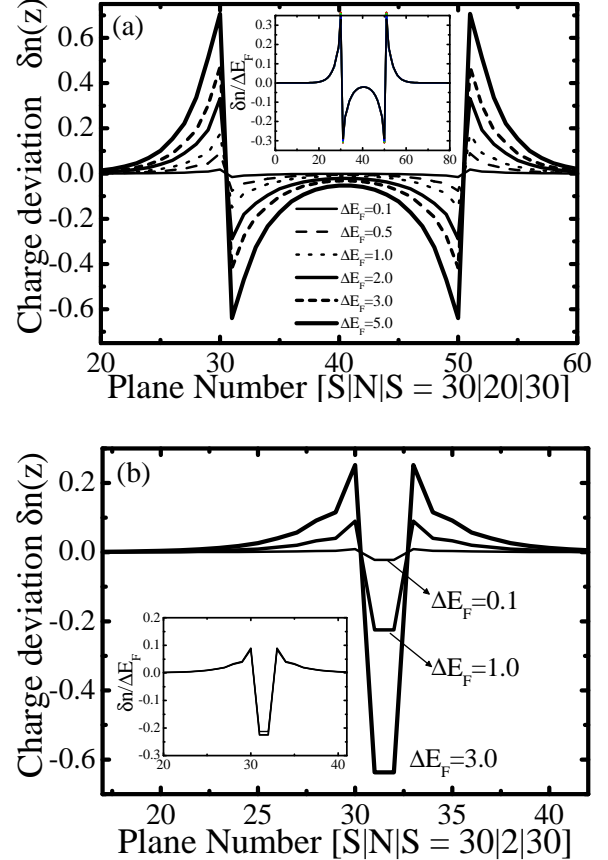


FIG. 3. Charge deviation $\delta n(z)$ (from half-filling) in SINIS junctions characterized by different Fermi level mismatches $\Delta E_F = E_F^N - E_F^S$. The N interlayer consists of: (a) 20 normal planes (b) 2 normal planes. The inset shows that distributions of $\delta n(z)$ for different ΔE_F can be rescaled to a single curve after multiplying them by the ratio $(\Delta E_F)_{\text{ref}} / \Delta E_F$, where $(\Delta E_F)_{\text{ref}} = 1.0$ is chosen as the reference distribution.

The corresponding local self-energy is given by the matrix

$$\hat{\Sigma}(\mathbf{r}_i, i\omega_n) = \begin{pmatrix} \Sigma(\mathbf{r}_i, i\omega_n) & \phi(\mathbf{r}_i, i\omega_n) \\ \phi^*(\mathbf{r}_i, i\omega_n) & -\Sigma^*(\mathbf{r}_i, i\omega_n) \end{pmatrix}. \quad (3)$$

The diagonal and off-diagonal (i.e., normal and anomalous) Green functions are defined, respectively, as

$$G(\mathbf{r}_i, \mathbf{r}_j, i\omega_n) = - \int_0^\beta d\tau \exp(i\omega_n \tau) \langle T_\tau \hat{c}_{j\sigma}(\tau) \hat{c}_{i\sigma}^\dagger(0) \rangle, \quad (4)$$

$$F(\mathbf{r}_i, \mathbf{r}_j, i\omega_n) = - \int_0^\beta d\tau \exp(i\omega_n \tau) \langle T_\tau \hat{c}_{j\uparrow}(\tau) \hat{c}_{i\downarrow}(0) \rangle, \quad (5)$$

where T_τ denotes time-ordering in τ and $\beta = 1/T$. The self-energies and Green functions are coupled together through the Dyson equation,

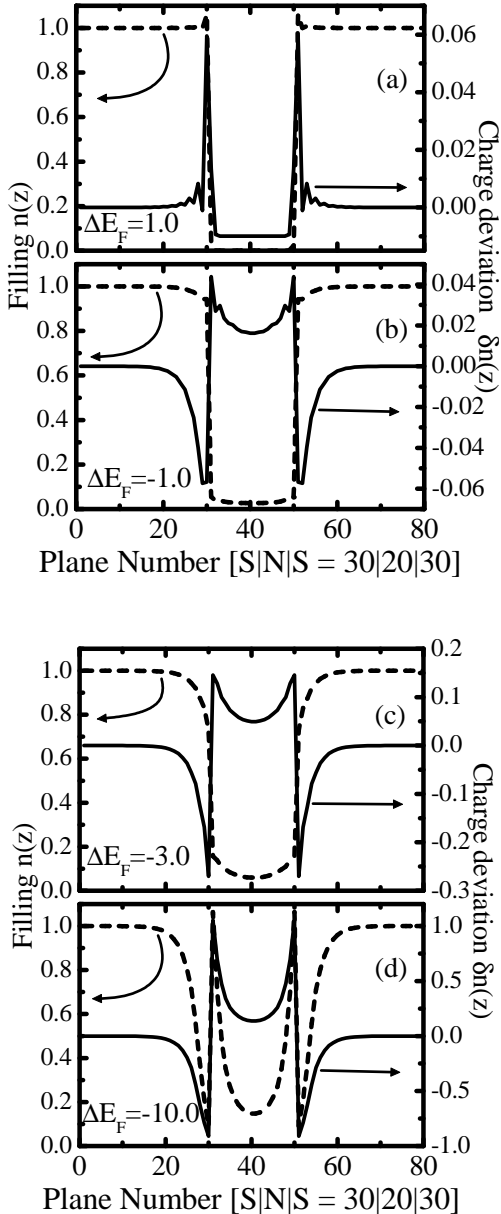


FIG. 4. Electron filling $n(z)$ [dashed line] and charge deviation $\delta n(z)$ [solid line] of a $SINIS$ Josephson junction with a thickness $L = 20a$ and the N interlayer chosen to approximate a highly doped semiconductor. The charge deviation is measured with respect to the equilibrium filling in the bulk, $n_S = 1$ in the superconductor and $n_N = 0.01$ in the normal region. The Fermi energy mismatch $\Delta E_F = E_F^N - E_F^S$ between the N and the S is: (a) $\Delta E_F = 1.0$, (b) $\Delta E_F = -1.0$, (c) $\Delta E_F = -3.0$, and (d) $\Delta E_F = -10.0$. The charge profile is virtually independent of temperature, both above and below T_c .

$$\hat{G}(\mathbf{r}_i, \mathbf{r}_j, i\omega_n) = G^0(\mathbf{r}_i, \mathbf{r}_j, i\omega_n) + \sum_l G^0(\mathbf{r}_i, \mathbf{r}_l, i\omega_n) \hat{\Sigma}(\mathbf{r}_l, i\omega_n) \hat{G}(\mathbf{r}_l, \mathbf{r}_j, i\omega_n), \quad (6)$$

where the local approximation for the self-energy, $\Sigma(\mathbf{r}_i, \mathbf{r}_j, i\omega_n) = \Sigma(\mathbf{r}_i, i\omega_n) \delta_{ij}$, is assumed. In the HFA

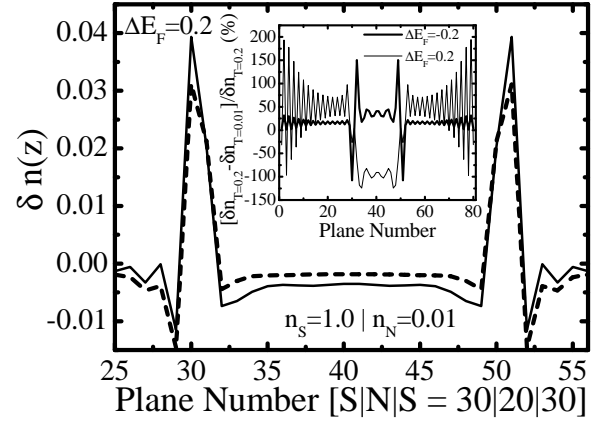


FIG. 5. Evolution of charge accumulation region in a $SINIS$ junction, with a highly doped semiconductor as the N interlayer ($n_N = 0.01$, $n_S = 1.0$, $\Delta E_F = 0.2$), upon crossing T_c of the S by going from $T = 0.2 = 1.8T_c$ to $T = 0.01 = 0.09T_c$. The inset shows the relative change of the charge deviation $[\delta n(z)_{T=0.2} - \delta n(z)_{T=0.01}] / \delta n(z)_{T=0.2}$ for two different charge redistributions: $\Delta E_F = 0.2$ and $\Delta E_F = -0.2$.

for the attractive Hubbard model, the local self-energy is found from the local Green function by

$$\Sigma(\mathbf{r}_i, i\omega_n) = U_i T \sum_{\omega_n} G(\mathbf{r}_i, \mathbf{r}_i, i\omega_n), \quad (7)$$

and

$$\phi(\mathbf{r}_i, i\omega_n) = -U_i T \sum_{\omega_n} F(\mathbf{r}_i, \mathbf{r}_i, i\omega_n). \quad (8)$$

The self-energy is time-independent because the interaction is instantaneous and we use the HFA (i.e., retardation effects in the superconductor are neglected). The noninteracting Green function, $G^0(\mathbf{r}_i, \mathbf{r}_j, i\omega_n)$ is diagonal in Nambu space, with an upper diagonal component given by

$$G^0(\mathbf{r}_i, \mathbf{r}_j, i\omega_n) = \int d^3\mathbf{k} \frac{e^{i\mathbf{k}\cdot(\mathbf{r}_i-\mathbf{r}_j)}}{i\omega_n + \mu - \varepsilon_{\mathbf{k}}}. \quad (9)$$

As all sites within a plane are identical, the self-energy need only be calculated once for each of the planes, while it is allowed to vary from plane to plane.

We work with Green functions $\hat{G}_{\alpha,\beta}(i\omega_n, k_x, k_y)$ represented in a mixed basis, which is defined by the two-dimensional momenta (k_x, k_y) and the (discrete) z -coordinate of the plane $\alpha = z_i/a$. This follows after the initial 3D problem is converted to a quasi-one-dimensional one⁴⁰ by performing a Fourier transformation within each plane (where the junction is translationally invariant) and retaining the real-space representation for the z -direction of the inhomogeneity. For the local interaction treated in the HFA, computation of the Green

function reduces to inverting an infinite block tridiagonal Hamiltonian matrix in real space. The Green functions are thereby evaluated as a matrix continued fraction (technical details are given elsewhere^{38,41}). The final solution is fully self-consistent in the order parameter $|\Delta(z)|e^{i\phi(z)}$ inside the part of the junction comprised of the N region and the first 30 planes inside the superconducting leads on each side of the N interlayer (see Fig. 1). The self-consistent region is long enough because $|\Delta(z)|$ heals to its bulk value over just a few coherence lengths ξ_0 . Our Hamiltonian formulation of the problem and its solution by this Green function technique is equivalent to solving a discretized version of the Bogoliubov-de Gennes³⁹ (BdG) equations in a fully self-consistent manner, i.e. by determining the off-diagonal pairing potential Δ_i in the BdG Hamiltonian³⁴ after each iteration until convergence is achieved. The tight-binding description of the electronic states also allows us to include an arbitrary band structure or unconventional pairing symmetry.³⁷

In conjunction with the self-consistent solution of the superconducting part of the problem, we have to self-consistently solve the electrostatic problem. Although both the S and N are half-filled in most of our calculations (i.e., there is no mismatch in the Fermi wave vector), shifting the bottom of the N band leads to a difference in their Fermi levels. This generates a redistribution of electrons around the SN interface when these are brought into contact. The resulting non-uniform electric field can be described by a potential $V(z)$ (for simplicity, we use the label z having in mind a discrete z_i coordinate at a particular site i) which varies in the transition layer around the SN boundary with a thickness of $2d$. In the region $z > |d|$ the following condition is satisfied

$$E_F^S + V(z < -d) = E_F^N + V(z > d) = \mu, \quad (10)$$

in order to ensure a constant electrochemical potential μ throughout the system in equilibrium. The solution which satisfies this equation is usually simplified²⁸ to $V(z) = V_0\delta(z) + \mu - v(z)$, where $v(z)$ is a monotonic function of z equal to E_F^S for $z < -d$ or E_F^N for $z > d$ (this allows one to formulate quasiclassical equations in the region $|z| > d$). Here we treat the contact between the S and N in a fully microscopic fashion: starting from the Hamiltonian (1), a Fermi level mismatch $\Delta E_F = E_F^N - E_F^S$, and assuming a screening length l_D of a few lattice spacings, we find the charge redistribution around the contact, as well as the corresponding classical electrostatic potential generated by them. Thus, our technique can treat arbitrary spatial variation of the (lattice) Green functions, superconducting order parameter, and electrostatic potential. This includes the region $|z| < d$, where we find a sharp increase of $V(z)$ but never as sharp as the (unphysical) delta function.

Since our *SINIS* multilayer structure is translationally invariant in the transverse direction, each infinite plane has a uniform surface charge distribution $\delta n(z)a$ which generates a homogeneous electric field $E(z) =$

$\delta n(z)a/2\epsilon_0\epsilon_\infty$ pointing along the z direction (ϵ_∞ is the relative dielectric constant of the ionic lattice). The quantum-mechanical part of the electrostatic problem entails determining the local electron density $n(z_i) \equiv n(z)$ (filling) at each site of a given plane $\alpha = z/a$

$$n(z) = k_B T \sum_{\omega_n} \int_{-\infty}^{\infty} \rho^{2D}(\varepsilon_{xy}) \operatorname{Im} G_{\alpha\alpha}(i\omega_n, \varepsilon_{xy}) d\varepsilon_{xy}, \quad (11)$$

where $\varepsilon_{xy} = -2t [\cos(k_x a) + \cos(k_y a)]$ is the in-plane kinetic energy for the transverse momentum (k_x, k_y) , and $\rho^{2D}(\varepsilon_{xy})$ is the two-dimensional tight-binding density of states on a square lattice (which is used for the sum over momenta parallel to the planes). The corresponding electric potential is determined classically from the “charge deviation” $\delta n(z) = n(z) - n$ (n is the average filling in the bulk, n_N or n_S)

$$\delta V(z) = -\frac{ea\delta n(z)|z - z'|}{2\epsilon_0\epsilon_\infty}. \quad (12)$$

This must be summed over all planes to give the on-site potential $V(z)$. Therefore, the small induced charge imbalance $\delta n(z) = N(\mu)e\delta V(z)$ satisfies (in a corresponding continuous system)

$$\frac{d}{dz}\delta n(z) = -\frac{e^2aN(\mu)}{2\epsilon_0\epsilon_\infty}\delta n(z) \quad (13)$$

where $N(\mu)$ is the total density of states at the chemical potential μ . This is integrated to give the distribution of the screened charge

$$\delta n(z) = \delta n(z_0) \exp\left[-\frac{e^2aN(\mu)}{2\epsilon_0\epsilon_\infty}(z - z_0)\right], \quad (14)$$

which decays exponentially on a length scale set by the Debye screening length

$$l_D = \left[\frac{e^2aN(\mu)}{2\epsilon_0\epsilon_\infty}\right]^{-1}. \quad (15)$$

Thus, the screening length is determined by $N(\mu)$ and ϵ_∞ (for example,³¹ $\epsilon_\infty = 20 - 30$ and $l_D = 5 - 10$ Å in high- T_c superconductors). We choose $\epsilon_\infty^S = \epsilon_\infty^N = 5.0$ which leads to $l_D \approx 3a$. The self-consistency in the electrostatic problem is required because $V(z)$ enters into the computation of the Green function as a diagonal potential in the Hamiltonian (1). The solution has converged when the potential is consistent with the charge distribution (11) determined from the Green function. Although this seems like a cumbersome computational task, the potential around the SN boundary barely changes when equilibrium Josephson current flows. Thus, the electrostatic part of the problem converges rapidly since the potential found in the solution at one phase gradient is

a good initial guess for the iteration scheme at the next superconducting phase gradient.

The density of electrons $n(z)$ on each site in a given plane (at zero supercurrent) is plotted as a function of the junction thickness for $\Delta E_F = 3.0$ in Fig. 2. The charge deviation $\delta n(z)$ from half-filling $n_S = n_N = 1$ and the corresponding electrostatic potentials are (approximately) symmetric around the SN boundary for thick enough junctions, as shown in Fig. 3. Strictly speaking, only such symmetric distributions should be denoted “screened dipole layers”. For thinner junctions, where the screening of the excess charge does not heal $n(z)$ to its equilibrium value, charge is depleted from the N interlayer. The example of this behavior is the $L = 2a$ junction in the lower panel of Fig. 3. It leads to a non-monotonic resistance as a function of junction thickness L at fixed ΔE_F (see Sec. IV). Thus, the charge effects become essential in short-coherence length superconducting junctions with thicknesses $L < 2l_D$, which are encountered in high- T_c grain boundaries.³¹

The interesting feature of the $\delta n(z)$ profiles for the half-filled S and N is that they can be approximately rescaled to a single reference distribution [set by $(\Delta E_F)_{\text{ref}}$] after multiplying each of them by the ratio $(\Delta E_F)_{\text{ref}}/\Delta E_F$, as shown in the insets of Fig. 3. We believe this occurs because the noninteracting cubic density of states is nearly constant close to half filling. The scaling becomes essential in computing the properties of junctions with large ΔE_F since one can use the scaled potential profile computed at a smaller ΔE_F as the initial guess in the iteration procedure. Since the $n_S = n_N = 1$ case has a higher degree of symmetry, we also perform calculations for $n_N = 0.01$ (which approximates a doped semiconductor) in the normal region and half-filling $n_S = 1.0$ in the superconductor. The result is shown in Fig. 4. Here the scaling of the $\delta n(z)$ distribution does not work as well (because the density of states has strong variation with energy). In addition, we find that the charge deviation is nonsymmetric, and yields a different $\delta n(z)$ for positive and negative ΔE_F [for symmetric filling $n_S = n_N$ the two distributions are simply related as $\delta n(z)|_{-\Delta E_F} = -\delta n(z)|_{\Delta E_F}$]. We also investigate the temperature dependence of the distributions of uncompensated charge for $T = 0.2$ (the chemical potential in the bulk N is $\mu = -5.566$ for $n_N = 0.01$) and at $T = 0.09$ (which is close to $T_c = 0.11$). In both cases $n_S = n_N = 1.0$ and $n_S \neq n_N = 0.01$ we find $\delta n(z)$ to be practically temperature independent (e.g., the change is at most 5% around the SN boundary) for ΔE_F shown in the previous figure. This feature is exploited in Sec. IV to calculate the normal state resistance of our junctions from an imaginary axis computation of the charge and potential profile in the superconducting state. However, for $n_S \neq n_N = 0.01$ and small $|\Delta E_F| \simeq 0.2$ a large change in the magnitude of $\delta n(z)$ is observed when going from $T = 0.2 > T_c$ to $T = 0.01 < T_c$, as shown in Fig. 5. Similar phenomenon has been found in the recent Raman studies³² which show a substantial change

in the thickness of the charge accumulation layer at the interface between Nb and InAs, as Nb undergoes a superconducting transition and proximity effects develop in the InAs layer. This would point to a proximity effect influenced screening length, which cannot be seen in our local (Thomas-Fermi) screening theory containing only two parameters which determine l_D : ϵ_∞ , which is fixed in our calculations, and the density of states $N(\mu)$ which can be modified by the proximity effect. Our observation of the change in the charge concentration above ($T \sim \Delta E_F$) and below T_c , without a palpable change in the screening properties, suggest that effects beyond the simple screening theory (e.g., nonlocal screening which becomes important in low filling cases³¹) probably have to be taken into account to understand this experiment.

III. SELF-CONSISTENT EQUILIBRIUM PROPERTIES OF SINIS JUNCTIONS

We first provide an insight into the microscopic properties of these junctions which are determined by the proximity effect that affects the critical current (in non-self-consistent calculations such effects are taken into account only through some effective phenomenological suppression parameter⁹). They are encoded in the self-consistently computed variation of the amplitude and phase of the order parameter $\Delta(z) = |\Delta(z)|e^{i\phi(z)}$ in the S or pair amplitude $F(z) = |F(z)|e^{i\phi(z)}$ in the N . These are related to each other inside the S by

$$\Delta(z) = -U(z)F(z). \quad (16)$$

where $F(z)$ is obtained as the equal-time limit of the local anomalous Green function introduced in Sec. II

$$F(z) = F(z_i, z_i, \tau = 0^+). \quad (17)$$

Although $\phi(z)$ and $F(z)$ are not directly measurable, they are important for understanding the superconductivity in inhomogeneous structures. Examples include the proximity effect in the N and the depression of $|\Delta(z)|$ (compared to its bulk value) on the S side of a SN boundary (“inverse proximity effect”). Since the critical current of the junction is determined by $\Delta(z)$ at the SN boundary, the study of $F(z)$ throughout the junction gives direct insight into how self-consistency affects the transport properties (analytical approaches usually assume a step function for $|\Delta(z)|$, which is applicable only for a limited range of junction parameters¹²). The non-zero value of $F(z)$ inside the superconductor results from the attractive pairing interaction $U(z) \neq 0$ [which also gives rise to the non-zero order parameter $\Delta(z)$]. In the normal metal, $U(z) = 0$ and the gap vanishes, but $F(z)$ can be non-zero due to the proximity effect. Therefore, it is more meaningful to plot $F(z)$, which is a continuous function throughout the junction. Inside the S , $F(z)$ should be understood as just $\Delta(z)/[-U(z)]$. The superconducting

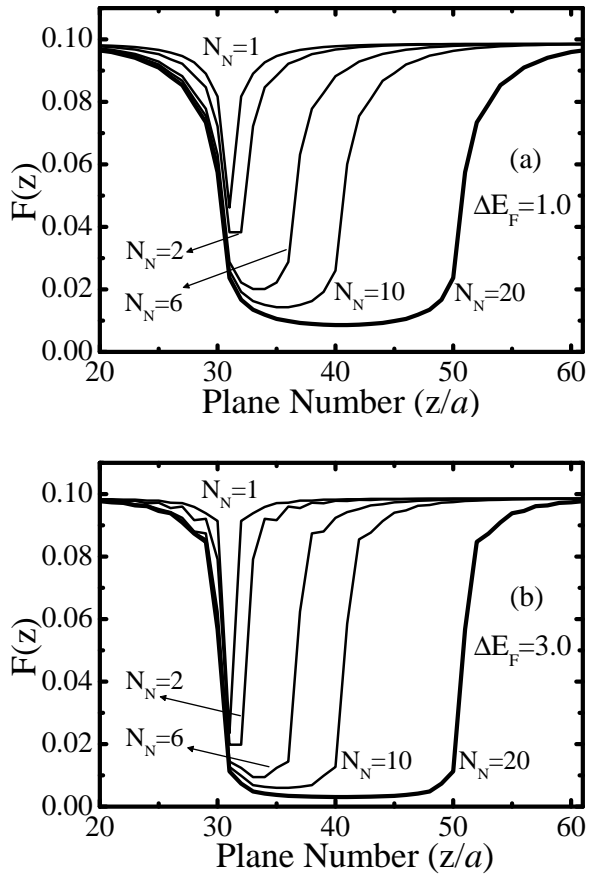


FIG. 6. Pair amplitude $F(z)$ at zero supercurrent flow in *SINIS* junctions of different thicknesses $L = N_N a$. The double-barrier structure arises from the charge inhomogeneity (see Fig. 2) induced by the difference between the Fermi energies of the normal metal and superconductor: (a) $\Delta E_F = E_F^N - E_F^S = 1.0$, and (b) $\Delta E_F = E_F^N - E_F^S = 3.0$.

correlations are imparted to the N region which is in contact with the S . They are described quantitatively by the pair amplitude⁴³ $F(z)$ (17). Because of the translational symmetry of the junction in the transverse direction, $F(z)$ is constant within the plane, and changes from plane to plane along z -axis. The scale over which $F(z)$ changes exponentially from the SN interface to zero in the bulk of the N is set by the normal metal coherence length ξ_N . However, as $T \rightarrow 0$ the length ξ_N diverges and the exponential decay of $F(z)$ crosses over to a slower power-law decay (like $1/z$ at $T = 0$, inside a N described by a Fermi liquid⁴⁴).

Although this description of the proximity effect has been used since the early days of inhomogeneous superconductivity studies,⁴³ it is only recently that mesoscopic superconductivity⁷ has established an explicit connection to a real-space picture of pairing correlations, provided by the phenomenon of (phase-coherent) Andreev reflection.¹¹ That $F(z)$ is non-zero in a normal region is equivalent to saying that the electron and an

Andreev reflected phase-conjugated hole maintain their single-particle phase coherence inside the N . Technically, this interpretation follows directly from the expression for $F(z)$ in terms of quasiparticle wave functions entering the BdG equations.⁶ In other words, near the SN boundary, Andreev reflection mixes electron-like and hole-like quasiparticles in the same proportion in which they are mixed in the S (where Bogoliubov quasiparticles are a mixture of electron-like and hole-like states with weights determined by the self-consistency condition) due to purely kinematic effects, since the interaction is absent in the N . The definition of $F(z)$ from Eqs. (2) and (17) in the second-quantized formalism, shows that such correlations can be interpreted alternatively as a condensate wave function leaking into the normal metal through the presence of evanescent Cooper pairs.⁴⁵ In the case of a Josephson junction, the overlap of two condensate wave functions provides a weak coupling between the superconducting leads, while insuring the global phase coherence and equilibrium current flow (i.e., the DC Josephson effect) for the time-independent phase difference between them. Thus, the two apparently different pictures of the Josephson effect in weak links (leakage of Cooper pairs versus Andreev reflection induced transfer of Cooper pairs) are in fact two facets of the same phenomenon.

We first show two examples of $F(z)$ computed self-consistently for vanishing supercurrent throughout the *SINIS* junction with $n_S = n_N = 1$. Figure 6 plots the scaling of $F(z)$ with the junction thickness for the I layers at the SN boundary being SDLs whose height is determined by $\Delta E_F = 1.0$ or $\Delta E_F = 3.0$. The shape of $F(z)$ evolves with the thickness, as well as with the height of the double-barrier. This second point is demonstrated in Fig. 7 where we fix L and vary the strength of the SDL barrier. Here one would expect the evolution of $F(z)$ toward a step function, which then justifies the use of rigid boundary conditions for strong enough scattering at the I barriers.¹² However, we find a non-monotonic change in the shape of $F(z)$: the influence of a SDL on the order parameter $\Delta(z)$ is first reduced with increasing ΔE_F , but then leads to a depressed $\Delta(z)$ near the boundary for a strong charge imbalance generated by $\Delta E_F = 10.0$. Since our previous results for a *SINIS* junction having a strong on-site Coulomb potential, confined within a single plane, exhibit a step function like³⁸ $\Delta(z)$, the effects observed here can be attributed to the finite spatial extent of the SDL. Moreover, we find that the step function (up to tiny oscillations near the boundary) for $\Delta(z)$ does develop in the special case of low filling in the N region, like $n_N = 0.01$, and a small mismatch $|\Delta E_F| \lesssim 1$. A specific example of this behavior (compared to the case with the same parameters, but with a negative ΔE_F) is shown in Fig. 8.

In the short junction case, the oscillations of Δ on the scale of λ_F are observed for large enough ΔE_F . In this case, as discussed in the previous section, the junction is too thin for the distribution of charge to heal to its

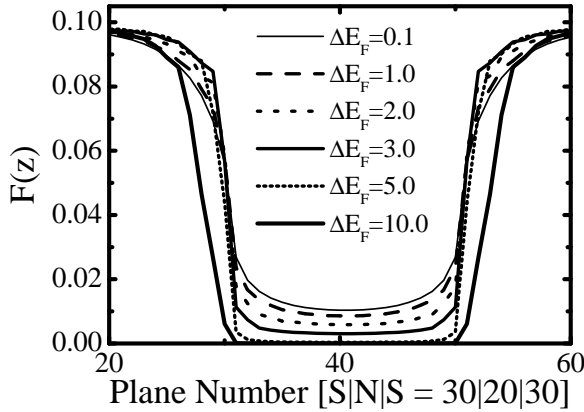


FIG. 7. Pair amplitude $F(z)$ at zero supercurrent flow in $SINIS$ junctions of thickness $L = 20a$ characterized by different heights of the SDL barriers. The double-barrier structure (charge inhomogeneity from Fig. 3) arises from the difference in Fermi energies of the normal metal and superconductor, $\Delta E_F = E_F^N - E_F^S$.

equilibrium value. The charge depletion inside the N brings it close to an insulating state. While oscillations on the scale of λ_F have been observed³⁴ in similar self-consistent calculations at $T = 0$ (and attributed to the mesoscopic coherence of a single particle wave function), here it appears that they are a property of the superconducting interface which terminates at an “insulator” (this is also exhibited by a thick junction with small n_N in Fig. 8). We have recently found such behavior, in its most pronounced form, in the case of SIS junctions, with I being a correlated insulator.⁴¹ In the self-consistent calculations one can also observe how $F(z)$ evolves, becoming smaller inside the N region, as the phase change across the interlayer is increased and the Josephson current approaches I_c . An example of such an effect due to self-consistency is shown in Fig. 9.

When self-consistency is satisfied, the phase of the order parameter $|\Delta(z)|e^{i\phi(z)}$ is not a constant inside the S leads (see also Sec. IV) because a phase gradient is needed to support the current in the S ensuring current conservation throughout the junction. Thus, the change of phase from plane to plane has to be extracted from the self-consistent solution for $|F(z)|e^{i\phi(z)}$. It can be expressed as the sum of a linear term and a “phase deviation” term $\delta\phi(z)$

$$\phi(z) = z \left(\frac{d\phi}{dz} \right)_{\text{bulk}} + \delta\phi(z), \quad (18)$$

where the distance z is measured from the origin along the z -axis. The linear term is determined by the phase gradient $(d\phi/dz)_{\text{bulk}}$ which is set as the boundary condition in the bulk of the superconductor. The non-trivial information contained in $\phi(z)$ is revealed by plotting $\delta\phi(z)$. The overall phase $\phi(z)$ increases smoothly and monotonically across the self-consistent region. We plot

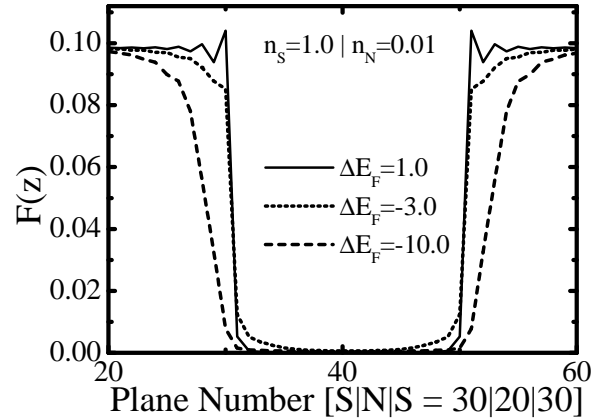


FIG. 8. Pair amplitude $F(z)$ at zero supercurrent flow in $SINIS$ junctions with thickness $L = 20a$. The double-barrier structure arises from the inhomogeneous charge redistributions, plotted in Fig. 4, induced by $\Delta E_F = E_F^N - E_F^S$ between the normal region with $n_N = 0.01$ and the superconductor at half-filling $n_S = 1$.

$\delta\phi(z)$ for two different junction thicknesses with $\Delta E_F = 1$ in Fig. 10. In general, oscillations of $\delta\phi(z)$ on the scale of λ_F are found for moderate ΔE_F and long enough junctions ($L \gtrsim 6a$). Oscillations, of both the phase and the order parameter, were found inside a long mesoscopic constriction in previous self-consistent calculations³⁴ at zero temperature (that gradually disappear with increasing T). Here we see the oscillations of $\delta\phi(z)$ at low temperature (but still $L < \xi_N$), while the corresponding $|F(z)|$ (Fig. 6) does not oscillate.

IV. CRITICAL CURRENTS AND CHARACTERISTIC VOLTAGES

In the self-consistent treatment, equilibrium supercurrent flows through the junction when the phase gradient $(d\phi/dz)_{\text{bulk}}$ exists in the bulk of the superconductor and a total phase change ϕ is established across the normal region. Therefore, we first find the solution for the bulk superconductor in both the absence of a supercurrent and in the presence of a supercurrent generated by a uniform variation in the order-parameter phase. The uniform bulk solution is then employed to provide the “boundary conditions” for the junction beyond the region where we determine properties self-consistently. Thus, our method does not require any assumptions about the boundary conditions at the interface between the barrier and the superconductor, which follow from the requirements of self-consistency.³⁸ We use current conservation as a stringent test of the achieved self-consistency in the solution for the Green function. Namely, the self-consistently determined $\Delta(z)$ ensures that Andreev reflection at each SN boundary generates supercurrent flow in the S leads (besides being responsible for the proximity effect in

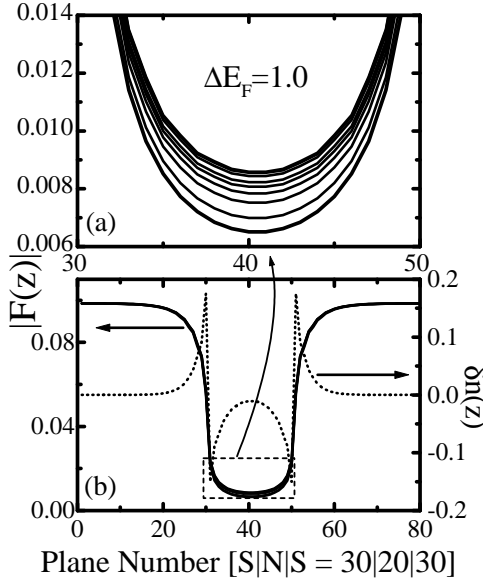


FIG. 9. Pair amplitude $|F(z)|$ at different supercurrent flows through the *SINIS* junction as a response to a non-zero phase gradient in the bulk and corresponding phase change ϕ across the N region. The thickness of the junction is $L = 20a$, and the two SDLs are generated by the Fermi energy mismatch $\Delta E_F = 1.0$ between the N and S , which are both at half filling. Panel (a) is a blow up of the dashed square region in panel (b).

the N discussed in Sec. II). Thus, the fulfillment of the self-consistency condition (16) means that the ‘‘source term’’ (on the right-hand side) vanishes in the equation of motion for the charge density operator \hat{n}_i

$$\frac{\partial \hat{n}_i}{\partial t} + \sum_j I_{ij} = \frac{2ie}{\hbar} \left(\Delta_i \langle c_{i\uparrow} c_{i\downarrow} \rangle - \Delta_i^* \langle c_{i\downarrow}^\dagger c_{i\uparrow}^\dagger \rangle \right), \quad (19)$$

thereby recovering current continuity at every site (I_{ij} is the current between two neighboring sites). When the current inside the superconductors is small, e.g., due to the geometrical dilution of a weak link with a junction area much smaller than ξ_0^2 , or when the junction resistance is dominated by a large interlayer resistance,^{6,12} one usually neglects the supercurrent flow and corresponding phase gradient in the bulk superconductor necessary to support it. Strictly speaking, such approaches violate current conservation.^{35,36} Inasmuch as our S and N layers have the same area, I_c/I_c^{bulk} can be close to one for thin junctions with weak SDLs at small ΔE_F . In such cases, current flow affects appreciably the superconducting order parameter [i.e., $F(z)$ both inside and outside of the N , cf. Sec. III] and a self-consistent treatment becomes necessary (as is the case for the critical current of the bulk superconductor⁴²). Because of the presence of a phase gradient inside the S , the simple picture¹ of an equilibrium current being related to the phase difference $\phi_L - \phi_R$ between the left and right S leads (where ϕ_L and ϕ_R are constant within the leads) is not applicable. Nevertheless, the solution for the current turns out

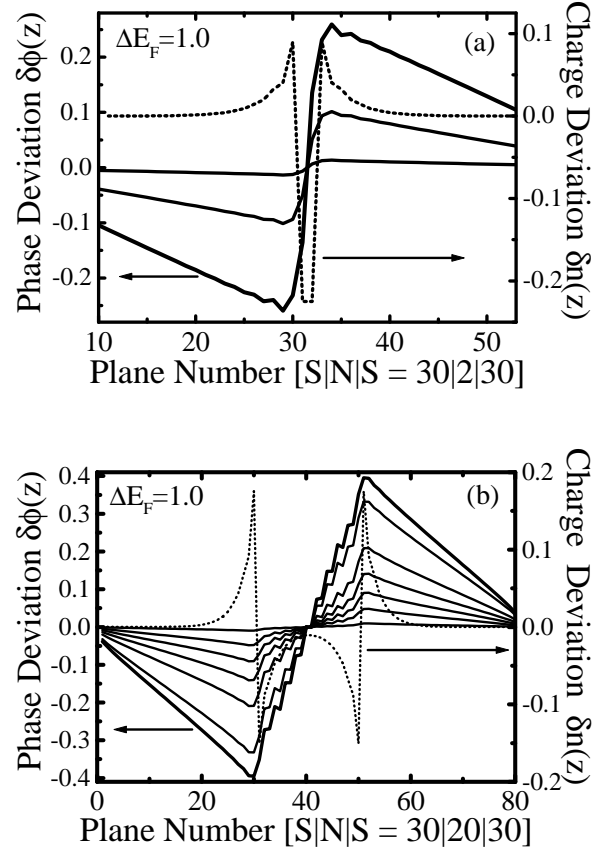


FIG. 10. Phase deviation $\delta\phi(z)$ [the total phase change along z -axis is the sum of the bulk phase gradient and $\delta\phi(z)$, Eq. (18)], within the self-consistently modeled part of the *SINIS* junction, at different supercurrent flows (the last curve corresponds to I_c). The thicknesses of the junctions are: (a) $L = 2a$, and (b) $L = 20a$, and the double-SDL-barrier (Fig. 3) is induced by the Fermi energy mismatch $\Delta E_F = 1.0$ between the N and S .

to be uniquely parameterized by a single quantity which can be taken as the phase change across the N region⁴⁶ (the other option is the phase offset³⁵ which is related to the phase change by a nontrivial scale transformation). In a discrete model like ours, a convention has to be introduced on how this change is extracted from $\phi(z)$ in Eq. (18). The thickness of the junction is defined to be the distance measured from the point z_L , in the middle of the last S plane on the left (at z_L^S) and the first adjacent N plane (at $z_L^N = z_L^S + 1$), to the middle point z_R between the last N and first S plane on the right (cf. Fig. 1). Since $\phi(z)$ is defined within the planes, we set $\phi(z_L) = [\phi(z_L^S) + \phi(z_L^N)]/2$ to be the phase at z_L , and equivalently for $\phi(z_R)$. The phase change across the barrier is then given by

$$\phi = \phi(z_R) - \phi(z_L) = L \left(\frac{d\phi}{dz} \right)_{\text{bulk}} + \delta\phi(z_R) - \delta\phi(z_L), \quad (20)$$

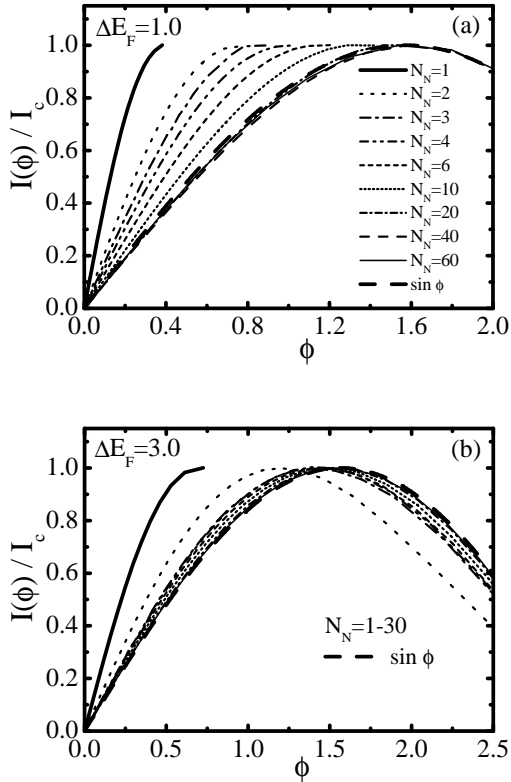


FIG. 11. Scaling of the current-phase relation $I(\phi)/I_c$ with the thickness of the SINIS junctions where the SDLs are determined by: (a) $\Delta E_F = 1.0$, and (b) $\Delta E_F = 3.0$. Note that the phase change ϕ_c at the critical current $I_c = I(\phi_c)$ varies nonmonotonically with the junction thickness, as shown in Fig. 12. The standard $I(\phi)/I_c = \sin \phi$ dependence in the *SIS* tunnel junction¹ is plotted as a reference only (which is analytically predicted for SINIS junctions with small barrier transparency at high enough temperatures⁹).

for a junction of thickness L . The current-phase relation $I(\phi)$ is obtained by computing the current for a fixed bulk phase gradient and associating this value with the phase change across the N region, which is extracted from the self-consistent pair amplitude $F(z) = |F(z)|e^{i\phi(z)}$. On the lattice, transport is described by the current across a link between two adjacent planes α and $\alpha + 1$. This current (per a^2) is obtained from the Green function connecting two neighboring planes as³⁸

$$I_{\alpha, \alpha+1} = \frac{2e\alpha t}{\hbar} k_B T \sum_{\omega_n} \int_{-\infty}^{\infty} \rho^{2D}(\varepsilon_{xy}) \times \text{Im} [G_{\alpha, \alpha+1}(i\omega_n, \varepsilon_{xy})] d\varepsilon_{xy}. \quad (21)$$

The first iteration in our self-consistent algorithm usually gives a current which is smaller inside the N than in the S region. The iteration cycle is completed when the current is constant throughout the junction. The only approximation invoked here is the presence of a (typically small) discontinuity in the supercurrent at the

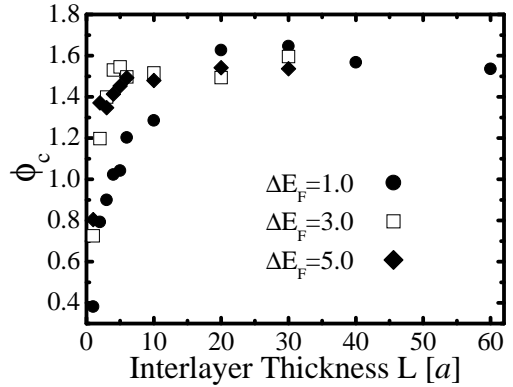


FIG. 12. Phase change ϕ_c at the critical current $I(\phi_c) = I_c$ plotted against the thickness of the SINIS junctions, where the double-SDL-barrier is determined by $\Delta E_F = 1.0$ (circles), $\Delta E_F = 3.0$ (squares), and $\Delta E_F = 5.0$ (diamonds).

bulk-superconductor/self-consistent-superconductor interface. We find that the superconducting order has always healed to its bulk value at that point. However, sometimes there can be a jump in $\phi(z)$ at this boundary when one nears the critical current. This discontinuity in the phase corresponds to a breakdown of current conservation at the this interface (it can become large for large ΔE_F and a thick junction, especially when one lies on the decreasing current side of the current-phase diagram). The critical current I_c of the junction is reached when the planes with the lowest pair amplitude $|F(z)|$ (which are located in the center of the N) can no longer support the necessary phase gradient to maintain current continuity.

The scaling of the shape of the current-phase relation with the junction thickness is plotted in Fig. 11 for different ΔE_F . We find large deviations from the usual sinusoidal $I(\phi)$ dependence for thin junctions and moderate heights of the SDL barriers. While in such cases (and at low temperatures) analytical predictions^{4,9,20} also give non-sinusoidal $I(\phi)$, our “critical” phase change ϕ_c [$I(\phi_c) = I_c$] is always below the analytical prediction $\phi_c \approx 1.86$ (Fig. 12), which can be attributed to the effects of self-consistency³⁵ (the other important distinction is that SDLs are spatially extended barriers). For thicker junctions, with high SDL barriers (and at high enough temperatures) the recovery of the usual *SIS* junction $I(\phi) = I_c \sin \phi$ current-phase relation is predicted.⁹ Here we find a current-phase relation $I(\phi)$ which is close to sinusoidal in the thick junction limit [(a) panel in Fig. 11], or in thin junctions with high SDL barriers [(b) panel in Fig. 11]. The corresponding critical current densities as a function of junction thickness are plotted in Fig. 13. For large ΔE_F , $I_c(L)$ is non-monotonic because of the special role played by the barriers formed in the junctions with $L < 2l_D$. When SDLs are completely screened inside the thick N interlayers, the decay of current is determined just by the exponential decay of the proximity

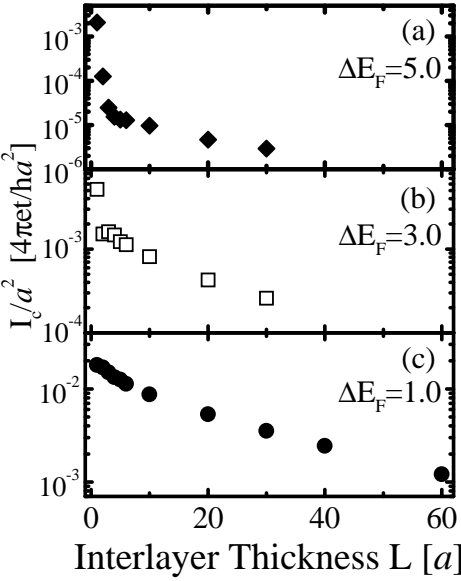


FIG. 13. Semilogarithmic plot of the critical current (per unit area a^2) as a function of junction thickness (i.e., number of planes $N_N = 1-60$ inside the N interlayer) of the *SINIS* junction for different SDLs determined by $\Delta E_F = E_F^N - E_F^S$. Both the S and N are at half-filling in the bulk.

coupling between the S leads through the clean normal interlayer (the resistance of these junctions is also practically independent of L , see Fig. 14). For example, the characteristic decay length, extracted from fitting^{12,47} $AL^p \exp[-L/\xi'_N]$ to $I_c(L)$ for $\Delta E_F = 1.0$ case in Fig. 13, is $\xi'_N \approx 35a \simeq \xi_N$ (with $p = 0.3$). For larger ΔE_F , and long enough junctions to ensure monotonic decay of $I_c(L)$, ξ'_N appears to be shorter.

We use a Kubo linear response formalism to determine the normal state resistance $R_N = 1/G_N$. Kubo theory is formulated in terms of the non-local conductivity tensor $\sigma(\mathbf{r}, \mathbf{r}'; \nu)$

$$\mathbf{j}(\mathbf{r}, \nu) = \int d\mathbf{r}' \sigma(\mathbf{r}, \mathbf{r}'; \nu) \cdot \mathbf{E}(\mathbf{r}', \nu), \quad (22)$$

which relates the current density $\mathbf{j}(\mathbf{r})$ to the electric field $\mathbf{E}(\mathbf{r})$ through a non-local Ohm's law (at finite frequency ν these are the respective Fourier components). Its physical meaning is obvious—it gives the current response at \mathbf{r} due to an electric field at \mathbf{r}' . Although an external electric field induces charges (and corresponding potentials) to linear order, the linear transport properties, like $\sigma(\mathbf{r}, \mathbf{r}')$, are found as the response to an external field only. This is because the current response to this inhomogeneous field (external + induced) is already beyond linear response.⁴⁹ Thus, only equilibrium screening has to be included in the Hamiltonian used to compute the Green function entering $\sigma(\mathbf{r}, \mathbf{r}')$ below.⁵⁰ This makes it possible to use the potential generated by the charge distributions $\delta n(z)$ (discussed in Sec. II), which is computed from the imaginary axis calculations, as an on-site fixed potential in the equilibrium Hamiltonian (1). In this way

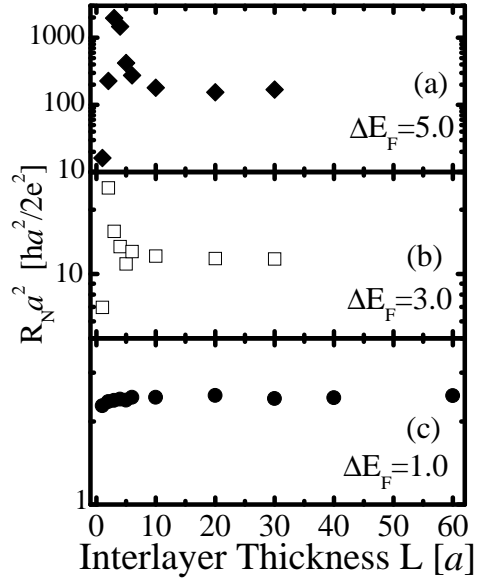


FIG. 14. Semilogarithmic plot of the normal state resistance (multiplied by the unit area a^2), as a function of the *SINIS* junction thickness, for different SDLs determined by $\Delta E_F = E_F^N - E_F^S$. Both the S and N are at half-filling in the bulk. Note that junctions with thickness smaller than $2l_D$ have charge depleted for large enough ΔE_F causing the resistance to change non-monotonically as a function of L . The Sharvin point contact resistance of the clean *SNS* junction (corresponding to $\Delta E_F = 0$ in our structure) is $R_{Sh}a^2 = 1.58ha^2/2e^2$

the potential of the SDLs enters the resistance calculation through the Green functions in Eq. (24) computed by real-axis analytic continuation. The DC conductance of the sample of volume Ω is expressed through $\sigma(\mathbf{r}, \mathbf{r}')$ as

$$\begin{aligned} G_N &= \frac{1}{V^2} \int_{\Omega} d\mathbf{r} \mathbf{E}(\mathbf{r}) \cdot \mathbf{j}(\mathbf{r}) \\ &= \frac{1}{V^2} \int_{\Omega} d\mathbf{r} d\mathbf{r}' \mathbf{E}(\mathbf{r}) \cdot \sigma(\mathbf{r}, \mathbf{r}') \cdot \mathbf{E}(\mathbf{r}'), \end{aligned} \quad (23)$$

where $\mathbf{E}(\mathbf{r})$ is the local field inside the sample and V is the externally applied voltage. Because of current conservation requirements on the form of⁴⁸ $\sigma(\mathbf{r}, \mathbf{r}')$, it is possible to use arbitrary electric field factors in Eq. (23) [including a homogeneous field $E = V/L$].

Since our system is effectively one-dimensional (in real space) we need to calculate the longitudinal component in the z -direction (perpendicular to the uniform planes) of $\sigma(z_i, z'_i)$. In a lattice model like ours, the relevant component of this tensor, $\sigma_{zz}(\alpha, \beta)$, is given by (neglecting vertex corrections)

$$\sigma_{zz}(\alpha, \beta) = \frac{-1}{k_B T} \frac{(eat)^2}{\hbar} \int_{-\infty}^{\infty} \rho^{2D}(\varepsilon_{xy}) d\varepsilon_{xy} \int_{-\infty}^{\infty} \frac{d\omega}{2\pi}$$

$$\begin{aligned} & \times [\text{Im } G_{\alpha,\beta+1}(\omega, \varepsilon_{xy}) \text{Im } G_{\beta,\alpha+1}(\omega, \varepsilon_{xy}) - \\ & \text{Im } G_{\alpha,\beta}(\omega, \varepsilon_{xy}) \text{Im } G_{\beta+1,\alpha+1}(\omega, \varepsilon_{xy})] \\ & \times [\cosh^2(\omega/2k_B T)]^{-1}, \end{aligned} \quad (24)$$

where $f(\omega)$ is the Fermi-Dirac distribution function. We first find the self-consistent solutions for the system in the normal state, with no current flowing, by setting the order parameter to zero on all planes. These solutions are then employed to calculate the Kubo tensor (24). The self-energy of the planes outside the interlayer contains only a constant real part, as the calculation is carried out within the HFA. Given the set of local self-energies, the Green functions which couple any two planes are readily found, for any momentum parallel to the planes.

The conductance G_N (per unit area a^2) of the lattice system is obtained from the discretized version of (23)

$$\frac{G_N}{a^2} = (R_N a^2)^{-1} = \sum_{\alpha,\beta} \sigma_{zz}(\alpha, \beta), \quad (25)$$

as the sum of the components of the non-local Kubo conductivity tensor. Thus, although one can find the inhomogeneous field³⁸ $E_{\beta,\beta+1}$ (across all links connecting planes β and $\beta+1$) by inverting the discretized version of Eq. (22), $I_{\alpha,\alpha+1} = a \sum_{\beta} \sigma_{zz}(\alpha, \beta) E_{\beta,\beta+1}$ for $I_{\alpha,\alpha+1}$ a constant throughout the system, the final expression for the conductance does not contain this field. The normal state resistances calculated in this framework are plotted in Fig. 14. In thin junctions and for large enough ΔE_F , a charge depletion layer arises inside the N which leads to a non-monotonic behavior of R_N (e.g., R_N increases sharply for $L = 2a$ and $\Delta E_F = 3.0$, or $L = 3a$ and $\Delta E_F = 5.0$). On the other hand, for small enough $\Delta E_F \lesssim 1.0$ the conductance is only slightly changed from the Sharvin point contact conductance⁵¹ of a ballistic SNS junction per unit area a^2 , $R_N a^2 = [(2e^2/h)(k_F^2/4\pi)]^{-1} \approx 1.58ha^2/2e^2$. Therefore, comparison of Fig. 13 and Fig. 14 shows that the SDL depresses the current substantially, while only weakly increasing the resistance. This reduces the $I_c R_N$ product, plotted in Fig. 15, thus showing that charge accumulation layers are detrimental to junction performance in electronics circuits. This is further confirmed by the fact that $I_c R_N$ in most of these junctions is below the product of the bulk critical current and the Sharvin point contact resistance $I_c^{\text{bulk}} R_{\text{Sh}} = 1.45\Delta/e$, which is the upper limit of the characteristic voltage in a clean SNS weak link (the SNS junction made of the same S leads as studied here, but with a dirty N interlayer, exhibits $I_c R_N > I_c^{\text{bulk}} R_{\text{Sh}}$, for some range of parameters⁴¹). Therefore, the SDL induced scattering on a SN boundary is one of the mechanisms which can account for the low $I_c R_N$ products observed in experiments³³ on nominally ballistic short SNS junctions (where R_N , being determined by the thin charge layer only, does not scale with L just like what happens in ballistic conductors). One way to test this conjecture is to use electron holography to map out

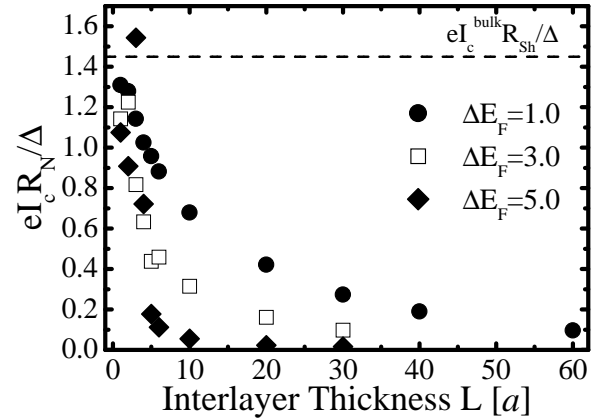


FIG. 15. Product of the critical current I_c and the normal state resistance R_N as a function of the $SINIS$ junction thickness, for different SDLs determined by $\Delta E_F = E_F^N - E_F^S$. Both the S and N are at half-filling in the bulk. The $I_c R_N$ is always below the product of the bulk critical current and Sharvin point contact resistance $I_c^{\text{bulk}} R_{\text{Sh}} = 1.45\Delta/e$ (dashed line), except in the case $L = 3a (\approx l_D)$ with $\Delta E_F = 5.0$.

the charge profile near the SN interface of these ballistic junctions.

V. CONCLUSIONS

We have studied the influence of a charge imbalance, that arises at the boundary between a short coherence length superconductor and a normal metal (due to Fermi energy mismatch) on the equilibrium properties of a $SINIS$ Josephson junction (where the S and N layers are of the same width). The screening length is large enough to generate a spatially extended charge redistribution that allows us to examine the interplay between the charge layer formation and superconductivity (characterized by the coherence length comparable to the screening length) near the SN boundary and in the N interlayer. This resembles the charge redistribution on the grain boundaries of a high- T_c superconductor. At half-filling in both the S and N , the charge distribution and its potential are symmetric (screened dipole layer), and can be rescaled to a single one determined by some reference Fermi level mismatch ΔE_F . When charge concentration in the N is a hundred times smaller than in the S , we find a proximity effect induced change in the charge redistribution generated by a small Fermi level mismatch upon moving from $T > T_c$ (where T is of the order of ΔE_F) to $T < T_c$.

The step-function-like order parameter (which is used in non-self-consistent approaches) is recovered only in the case of a low charge density in the N (compared to the filling in the S) and a small mismatch $|E_F^N - E_F^S| \lesssim 1$. The $SINIS$ junction exhibits unusual properties when its thickness is comparable to the screening length. While

the charge layer leads to a depression of the order parameter near the SN boundary, and thereby the junction critical current, it influences the normal state resistance in a much weaker fashion. Therefore, the I_cR_N product, relevant for digital electronics application, is reduced. This points out that such space-charge layers should be avoided to optimize junction performance and increase the critical current in high- T_c superconductors.⁵²

ACKNOWLEDGEMENTS

We are grateful to the Office of Naval Research for financial support from the grant number N00014-99-1-0328. Real-axis analytic continuation calculations were partially supported by HPC time from the Arctic Region Supercomputer Center. We have benefited from the useful discussions with A. Brinkman, J. Ketterson, T. Klapwijk, K. K. Likharev, J. Mannhart, I. Nevirkovets, N. Newman, I. V. Roshchin, J. Rowell, S. Tolpygo, and T. van Duzer.

- ¹ B. D. Josephson, Phys. Lett. **1**, 251 (1962).
- ² T. van Duzer and C. W. Turner, *Principles of Superconducting Devices and Circuits* (2nd ed., Prentice Hall, Upper Saddle River, 1999).
- ³ A. Kastalsky, A.W. Kleinsasser, L.H. Greene, R. Bhat, F.P. Milliken, and J.P. Harvison, Phys. Rev. Lett. **67**, 3026 (1991); A. W. Kleinssaser and A. Kastalsky, Phys. Rev. B **47**, 8361 (1993).
- ⁴ A. Brinkman and A. A. Golubov, Phys. Rev. B **61**, 11 297 (2000).
- ⁵ A. F. Volkov, Phys. Rev. Lett. **74**, 4730 (1995).
- ⁶ C. W. J. Beenakker, Rev. of Mod. Phys. **69**, 731 (1997).
- ⁷ Special issue of *Superlattices and Microstructures*, **25** No. 5/6 (1999).
- ⁸ M. Maezawa and A. Shoji, Appl. Phys. Lett. **70**, 3603 (1997).
- ⁹ For a review see: M. Yu. Kupriyanov, A. Brinkman, A. A. Golubov, M. Siegel, H. Rogalla, Physica C **326-327**, 16 (1999).
- ¹⁰ A. Brinkman, A. A. Golubov, H. Rogalla, and M. Kupriyanov, Supercond. Sci. Technol. **12**, 893 (1999); D. Balashov, F.-Im. Buchholz, H. Schulze, M. I. Khabipov, R. Dolata, M. Yu. Kupriyanov, and J. Niemeyer, Supercond. Sci. Technol. **12**, 244 (2000).
- ¹¹ A. F. Andreev, Zh. Eksp. Teor. Fiz. **46**, 1823 (1964) [Sov. Phys. JETP **18**, 1228 (1964)].
- ¹² K. K. Likharev, Rev. Mod. Phys. **51**, 101 (1979).
- ¹³ M. B. Ketchen, IEEE Trans. Magn. **27**, 2916 (1991).
- ¹⁴ K. K. Likharev and V. K. Semenov, IEEE Trans. Appl. Supercond. **1**, 1 (1991).
- ¹⁵ M. Gurvitch, M. A. Washington, and H. A. Huggins, Appl. Phys. Lett. **42**, 472 (1983).

- ¹⁶ A. W. Kleinsasser, A. C. Callegari, B. D. Hunt, C. Rogers, R. Tiberio, and R. A. Buhrman, IEEE Trans. Magn. **17**, 307 (1981).
- ¹⁷ A. Zehnder, Ph. Lerch, S. P. Zhao, Th. Nussbaumer, E. C. Kirk, and H. R. Ott, Phys. Rev. B **59**, 8875 (1999).
- ¹⁸ L. G. Aslamasov, A. I. Larkin, and Yu. N. Ovchinnikov, Sov. Phys. JETP **28**, 171 (1969).
- ¹⁹ W. Belzig, F.K. Wilhelm, C. Bruder, G. Schön, and A.D. Zaikin, Superlattices and Microstructures **25**, 1251 (1999).
- ²⁰ M. Yu. Kupriyanov and V. F. Lukichev, Sov. Phys. JETP **67**, 1163 (1988).
- ²¹ G. E. Blonder, M. Tinkham, and T. M. Klapwijk, Phys. Rev. B **25**, 4515 (1982).
- ²² A. Furusaki, H. Takayanagi, and M. Tsukada, Phys. Rev. B **45**, 10 563 (1992).
- ²³ A. Chrestin, T. Matsuyama, and U. Merkt, Phys. Rev. B **59**, 498 (1994).
- ²⁴ G. Johansson, E. N. Bratus', V. S. Shumeiko, and G. Wendin, Phys. Rev. B **60**, 1382 (1999).
- ²⁵ I. P. Nevirkovets and S. E. Shafranjuk, Phys. Rev. B **59**, 1311 (1999).
- ²⁶ M.A.M. Gijs and G.E.W. Bauer, Adv. Phys. **46**, 286 (1997), and references therein.
- ²⁷ V. K. Dugaev, V. I. Litvinov, and P. P. Petrov, Phys. Rev. B **52**, 5306 (1995).
- ²⁸ A. V. Zaitsev, Zh. Eksp. Teor. Fiz. **86**, 1742 [Sov. Phys. JETP **59**, 1015 (1985)].
- ²⁹ K. A. Delin and A. W. Kleinsasser, Supercond. Sci. Technol. **9**, 227 (1996).
- ³⁰ J. Mannhart and H. Hilgenkamp, Appl. Phys. Lett. **73**, 265 (1998).
- ³¹ A. Gurevich and E. A. Pashitskii, Phys. Rev. B **57**, 13 878 (1998).
- ³² I. V. Roshchin, A. C. Abeyta, L. H. Greene, T. A. Tanzer, J. F. Dorsten, P. W. Bohn, S.-W. Han, P. F. Miceli, and J. F. Klem, unpublished; I. V. Roshchin, Ph.D. thesis, *Electronic and optical properties of thin-film superconductors and superconductor-semiconductor interfaces*, Department of Physics, University of Illinois at Urbana-Champaign, Urbana (2000); L. H. Greene, J. F. Dorsten, I. V. Roshchin, A. C. Abeyta, T. A. Tanzer, G. Kuchler, W. L. Feldmann, P. W. Bohn, Czech. J. Phys. **46**, 3115 (1996).
- ³³ J.P. Heida, B.J. van Wees, T.M. Klapwijk, and G. Borghs, Phys. Rev. B **60**, 13 135 (1999), and references therein.
- ³⁴ A. Levy-Yeyati, A. Martín-Rodero, and F. J. García-Vidal, Phys. Rev. B **51**, 3743 (1995); J. C. Cuevas, A. Martín-Rodero, and A. Levy Yeyati, Phys. Rev. B **54**, 7366 (1996).
- ³⁵ F. Sols and J. Ferrer, Phys. Rev. B **49**, 15913 (1994).
- ³⁶ R. A. Reidel, L.-F. Chang, and F. Bagwell, Phys. Rev. B **54**, 16 082 (1996).
- ³⁷ A. M. Martin and J. F. Annett, in Ref. 7.
- ³⁸ P. Miller and J. K. Freericks, J. Phys.: Condens. Matter. **13**, 3187 (2001).
- ³⁹ P. G. de Gennes, *Superconductivity of Metals and Alloys* (Addison-Wesley, 1966).
- ⁴⁰ M. Potthoff and W. Nolting, Phys. Rev. B **59**, 2549 (1999).
- ⁴¹ J. K. Freericks, B. K. Nikolić, and P. Miller, cond-mat/0103067.
- ⁴² J. Bardeen, Rev. Mod. Phys. **34**, 667 (1962).
- ⁴³ G. Deutscher and P.G. De Gennes, in *Superconductivity*,

ed. by R.D. Parks, (Marcel Dekker, New York, 1969), Vol. II, p. 1005.

⁴⁴ D. S. Falk, Phys. Rev. **132**, 1576 (1963).

⁴⁵ G. B. Lesovik, T. Martin, and G. Blatter, cond-mat/0009193.

⁴⁶ M. Yu. Kupriyanov, Pis'ma Zh. Eksp. Teor. Fiz. **56**, 414 (1992) [JETP Lett. **56**, 399 (1992)].

⁴⁷ A. W. Kleinsasser and T. N. Jackson, Phys. Rev. B **42**, R8716 (1990).

⁴⁸ C. L. Kane, R. A. Serota, and P. A. Lee, Phys. Rev. B **37**, 6701 (1988).

⁴⁹ B. K. Nikolić and P. B. Allen, Phys. Rev. B **60**, 3963 (1999).

⁵⁰ A. D. Stone, in *Mesoscopic Quantum Physics*, edited by E. Akkermans, J.-L. Pichard, and J. Zinn-Justin, Les Houches, Session LXI, 1994 (North-Holland, Amsterdam, 1995)..

⁵¹ Yu. V. Sharvin, Zh. Eksp. Teor. Phys. **48**, 984 (1965) [Sov. Phys. JETP **21**, 655 (1965)].

⁵² A. Scheml, B. Goetz, R. R. Schulz, C. W. Schneider, H. Bielefeldt, H. Hilgenkamp, and J. Mannhart, Europhys. Lett. **47**, 110 (1999); G. Hammerl, A. Schmehl, R. R. Schulz, B. Goetz, H. Bielefeldt, C. W. Schneider, H. Hilgenkamp, and J. Mannhart, Nature **407**, 162 (2000).